Chemical routes to materials

Facile in situ growth of ZIF-8 films onto aluminum for applications requiring fast thermal response

Rocío L. Papurello[1] and Juan M. Zamaro[1,*]

[1] *Instituto de Investigaciones en Catálisis y Petroquímica, INCAPE (FIQ, UNL, CONICET), Santiago del Estero, 2829 (3000) Santa Fe, Argentina*

ABSTRACT

In this work, we report a simple approach for the synthesis of highly crystalline films of ZIF-8 directly grown onto non-functionalized common aluminum substrates through an easy, short in situ solvothermal methodology. Through several techniques such as XRD, SEM, EDS, AFM and XPS, it is shown that a simple, short pretreatment of the substrate with a dilute hydrochloric acid solution promotes the subsequent solvothermal nucleation and growth of continuous, homogeneous micrometer thickness and very adherent ZIF-8 films. The robustness and usefulness of ZIF-8/aluminum are shown by testing it in the highly exothermic catalytic reaction of carbon monoxide oxidation, in which it presented a high performance and durability, preserving the metal–organic framework integrity during reaction time. This behavior demonstrates that the novel ZIF-8/aluminum systems have a high potential for use in applications at moderate temperatures demanding a fast heat exchange rate between the metal–organic framework (MOF) film and the substrate.

 Springer

GRAPHICAL ABSTRACT
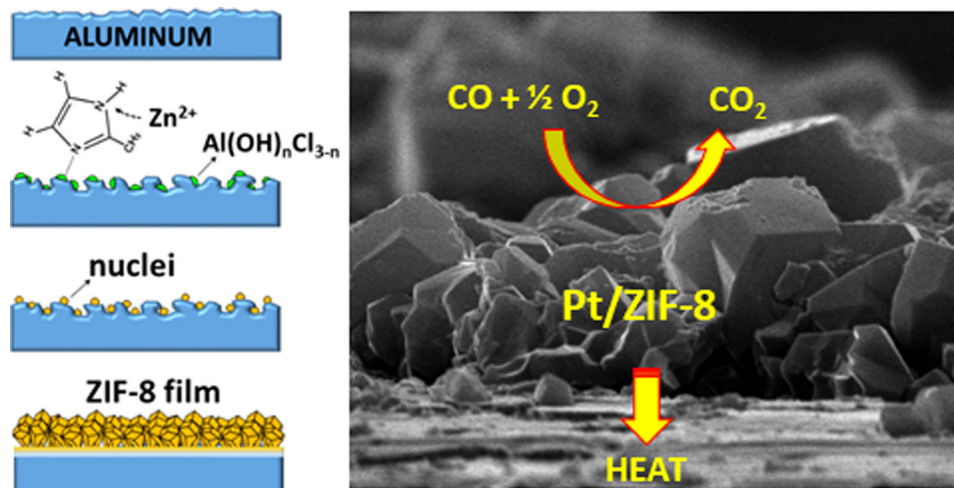
Introduction

Zeolitic imidazolate frameworks (ZIFs) constitute a family of metal–organic frameworks (MOFs) with uniform micropores interconnected by cavities, made up of a metal cation (e.g., Zn^{2+}, Co^{2+}) bound to nitrogen of methylimidazolate anions in a tetrahedral arrangement which generate a zeolite-type topology [1]. In particular, ZIF-8 is of interest for its use in various applied fields since it has a high specific surface area, thermal stability and chemical stability [2]. These qualities have sparked a growing interest in the research of ZIF-8 films. Particular attention has been given to these films employed mainly for separation membranes [3] which have been applied in H_2 purification [4], separation of alkanes/alkenes [5] or CO_2/CH_4 mixtures [6], among other uses. For this reason, the synthesis of ZIF-8 films has been carried out mostly on porous ceramic substrates, such as alumina [3]. However, it has also been obtained on other types of substrates to be applied as sensors or devices based on optical properties [7] including, among others, non-metallic substrates such as surface-modified glass [8], indium tin-oxide (ITO) glass [9], nylon [10], polymer [11], carbon nanotubes [12] or titania [13].

Several deposition techniques have been employed to obtain ZIF-8 films, such as layer-by-layer deposition [14], spin coating [9, 15], self-assembly of nanocrystals [16], Langmuir–Blodgett [17], chemical vapor deposition [18], supersonic cold spraying [19] and pulsed-laser deposition [20]. Another route is the solvothermal method, which allows obtaining strongly anchored and well inter-grown polycrystalline ZIF-8 films as has been shown on ceramic substrates [3, 7]. This technique is simple, widespread, does not require expensive equipment and allows manipulating some properties such as the microstructure or preferred crystal orientation of the films by controlling the synthesis parameters [7]. Nevertheless, the growth of ZIF-8 on metal substrates through the solvothermal method is hampered because of the low surface roughness and few surface functional groups of these substrates, which are mandatory for the nucleation step. ZIF-8 has been grown on macroporous stainless-steel meshes [21, 22], but a pre-functionalization of this substrate was required through a long contact with dopamine solution or by exposure to pure argon plasma followed by treatments with aminopropyltriethoxysilane (APTES), respectively. ZIF-8 films have also been obtained on zinc plates through a direct in situ conversion method [23], but it is limited only to the use of this metallic substrate. Furthermore, adherent ZIF-

8 films have been obtained on copper substrates through the secondary growth technique [24]. The dependence of the synthesis process of a MOF with the chemical nature of the substrate has meant that to date there are no reports of direct in situ solvothermal growth of ZIF-8 onto non-functionalized aluminum.

Aluminum is of technological interest because it has high thermal conductivity and thermal diffusivity [25], which is advantageous for its use as substrate in devices dedicated to applications involving a fast heat exchange. Some of the applications that could require a fast thermal response between the metal–organic framework film and the substrate can occur in the field of catalysis or adsorption processes, among others. This property, for example, would improve the heat conduction to or from the film for a quasi-isothermal operation of highly endo- or exothermic catalytic reactions [26] as have been shown with ZIF-8 film/copper-based microreactors [27]. ZIF-8/aluminum would also have impact on real adsorption processes in which a fast heat transfer rate between the film and the substrate is crucial for the optimal management of this exothermic process. It has recently been demonstrated that ZIF-8 films have heat transport ability [28] which is a key property in the development of technologies for the fast, efficient storage and release of natural gas or hydrogen [29]. Additionally, aluminum is low cost, easy to handle, has high strength/stiffness to weight ratio, versatility and is commercially available in a wide spectrum of geometrical shapes. Despite the above-discussed attractive utilities of ZIF-8/aluminum, a detailed analysis of the literature to date reveals only two articles on this topic, reported by Zhang et al. [30, 31], who synthesized ZIF-8 films onto aluminum plates for the purpose of corrosion protection barrier. They employed polished ultrapure aluminum plates pretreated for 24 h with a solution containing zinc and urea to obtain layered double hydroxide coatings of ZnAl-CO$_3$. Then, in a second step, the modified Al plate was subjected to another solvothermal step for 24 h to obtain a ZIF-8 growth.

The aforementioned highlights the need to carry out new studies toward the development of ZIF-8 films on aluminum substrates. With this objective, in the present work we report an easy and straightforward direct in situ growth of ZIF-8 films on aluminum through a direct solvothermal treatment of the substrate. This is the first report of a direct synthesis of a continuous and adherent film of ZIF-8 onto 1050-type aluminum foils of industrial use without surface pre-functionalization. Furthermore, such ZIF-8 films can be successfully used in applications requiring a strong demand of heat transfer between the MOF and the substrate as it is shown through the highly exothermic catalytic CO oxidation reaction.

Experimental

Substrate pretreatments

Common and low-cost 1050-type aluminum foils easily available from non-ferrous metal suppliers were used (50 μm thickness; Al 99.5%, Si 0.25%, Fe 0.40%, Cu 0.05%, Mn 0.05%, Mg 0.05%, Zn 0.05%, Ti 0.03%), which were cut in 2 × 2.5 cm pieces. To facilitate their further analysis in the catalytic application, some of them were micro-folded with a homemade device containing two rollers with micrometer-sized teeth. The substrates were first cleaned with water and then with acetone in an ultrasonic bath; afterward, they were subjected to pretreatments with NaOH or HCl solutions (5 wt.%) under magnetic stirring from 5 up to 30 min. Finally, they were washed with water in an ultrasonic bath for 15 min and dried with N$_2$.

In situ growth of ZIF-8 films

The synthesis of ZIF-8 films was carried out by a direct solvothermal treatment of the substrates employing a previously reported synthetic protocol that uses methanol as solvent [24]. (NO$_3$)$_2$Zn·6H$_2$O (Sigma-Aldrich, reagent grade 98.0%), sodium acetate (Cicarelli, pro-analysis), 2-methylimidazole (Sigma-Aldrich, 99.0%) and methanol (Cicarelli, pro-analysis) were used in 1:2:2:200 molar ratios, respectively. Methanolic solutions of 2-methylimidazole and zinc nitrate were prepared separately under stirring until the solids dissolved and were then mixed and maintained under stirring for another 20 min. After that, the solution was placed in a Teflon-lined autoclave together with the substrate which was positioned through a Teflon support, in vertical position. The solvothermal treatments were carried out at 120 °C for 10 h after which the samples were withdrawn and treated in an ultrasonic bath with water
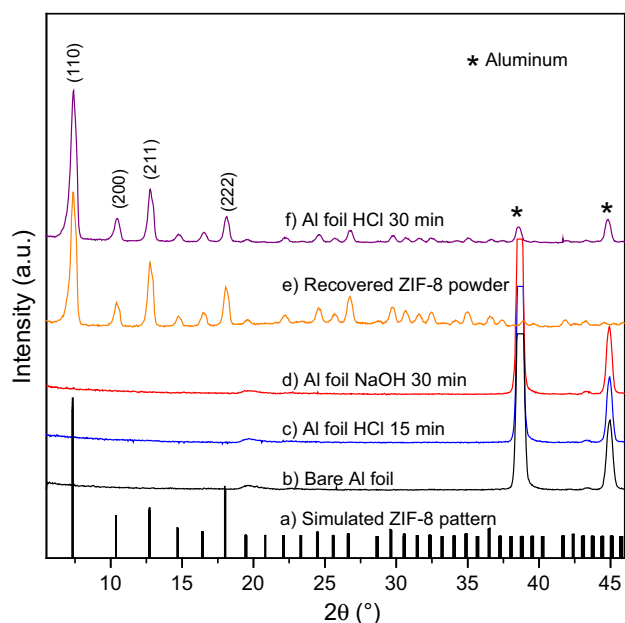
Figure 1 X-ray diffraction: (**a**) simulated pattern of ZIF-8 from its crystallographic file (CCD 602,538) using the Diamond 3.2 software. Substrates subjected to solvothermal treatments: (**b**) original substrate; (**c**) substrate pretreated with acid for 15 min; (**d**) substrate pretreated with base for 30 min; (**e**) recovered powder from the synthesis solution; (**f**) substrate pretreated with acid for 30 min.

for 30 s to remove loosely attached solids from the surface. Finally, the samples were dried in oven (120 °C, 24 h).

Activation of ZIF-8/Al films

To test the ZIF-8/Al films, they were activated by incipient wetness impregnation with ethanolic solutions of $Pt(NH_3)_4(NO_3)_2$ (Sigma-Aldrich, 99.9%). An exact volume of the solution was added dropwise on the films to obtain metal loads from 1 to 5 wt.%, and then, prior to the catalytic test, an in situ reduction was carried out in He or H_2 stream at 300 °C. These conditions were adopted taking into account reported data for the reduction of platinum precursors [32]. The systems were named Pt(x)/ZIF-8/Al, where x is the % wt. of Pt with respect to the mass of the MOF film.

Physicochemical characterization

X-ray diffraction (XRD) was performed with a Shimadzu XD-D1 instrument by scanning the 2θ angle at $2° min^{-1}$ between 5° and 50° (CuKα radiation, λ

1.5418 Å, 30 kV, 40 mA). The quality and microstructure of the substrates and films were examined by scanning electron microscopy (SEM) with a Phenom World ProX (Netherlands) benchtop instrument operated at 15 kV. Electron-dispersive spectroscopy (EDS) was performed with an equipment coupled to the SEM instrument. Thermogravimetric analysis (TGA) and single differential thermal analysis (SDTA) were conducted with a Mettler-Toledo STARe TGA/SDTA 851e module (25 to 600 °C, $10 °C min^{-1}$, air flow, $50 mL min^{-1}$). Diffuse reflectance infrared spectroscopy (DRIFT) was performed with a Shimadzu Prestige 8101 M (40 scans, resolution $4 cm^{-1}$). The substrate surface was examined by X-ray photoelectron spectroscopy (XPS) with a Multitechnique Specs module (pass energy of 30 eV with a Mg anode operated at 200 W). The peak of C 1 s at 284.8 eV was taken as internal reference, and the data processing was performed using the Casa XPS software. The substrate surface was also examined by atomic force microscopy (AFM) with an Agilent 5400 (Keysight Technologies) with a standard cantilever in intermittent contact-mode obtaining topography and phase images.

Catalytic characterization

Pt-ZIF8/Al films were tested in the CO oxidation reaction through a microreactor module connected to a continuous flow system in which reactant gases were dosed by mass flow controllers (Brooks Instruments 4800 series). The module was heated and controlled through a K-type thermocouple of 0.9 mm in diameter inserted 1 mm below the surface of the films. This was operated with a Delta B Series temperature controller programmer in PID mode, assuring a precise measurement and control of the temperature of the films during the reaction. The samples were first heated in He or H_2 flux $(20 mL min^{-1})$ up to 300 °C $(5 °C min^{-1})$ and maintained at that temperature for 2 h. After that, catalytic tests were performed with a molar gas feed composition of 1% CO, 2% O_2 in He balance with a total flow of $30 cm^3 min^{-1}$. The measurements were obtained after stabilizing the microreactor for 15 min at different temperatures. The CO conversions were determined by analyzing the gas exit with an on-line Shimadzu GC-2014 chromatograph equipped with a TCD detector and a 5A molecular sieve column.

Figure 2 SEM images of the aluminum substrate: (**a**, **b**) without treatment; (**c**, **d**) pretreated with acid for 15 min; (**e**, **f**) pretreated with acid for 30 min. Note: the images a, c, e were acquired at the same magnification (1000 X), whereas the images b, d, f were acquired at a higher magnification (5000 X).
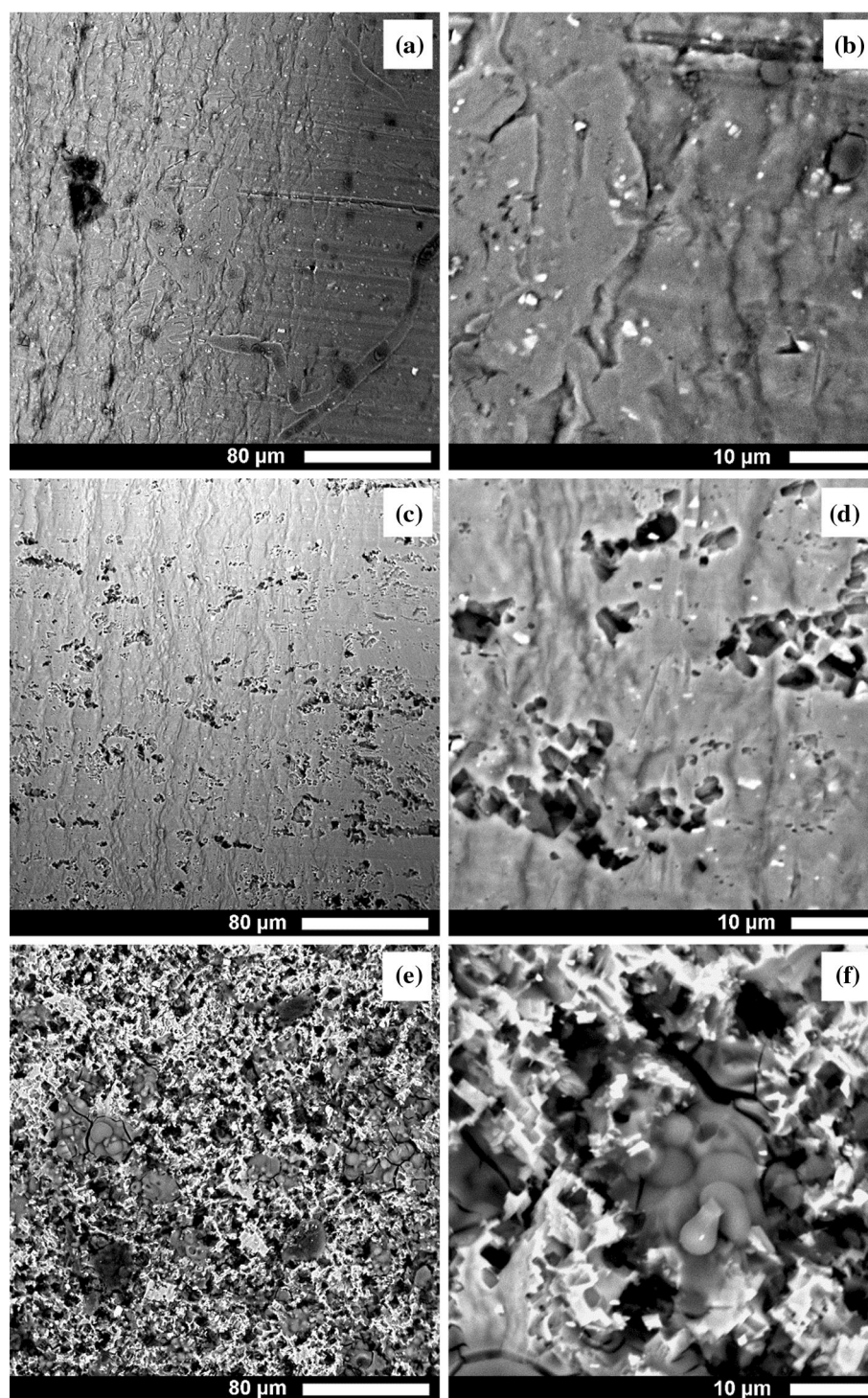
Results and discussion

Influence of the substrate pretreatment

When the solvothermal treatment of bare aluminum foil was carried out, the sample showed an XRD pattern with two intense signals at 2θ 38.5° and 44.8°, characteristic of the aluminum structure (JCPDS 4–787), while neither alumina nor ZIF-8 signals were detected (Fig. 1b). However, a highly crystalline solid was recovered from the synthesis solution (Fig. 1e) which presented all the indexed signals of ZIF-8, as shown in the simulated XRD pattern (Fig. 1a). This
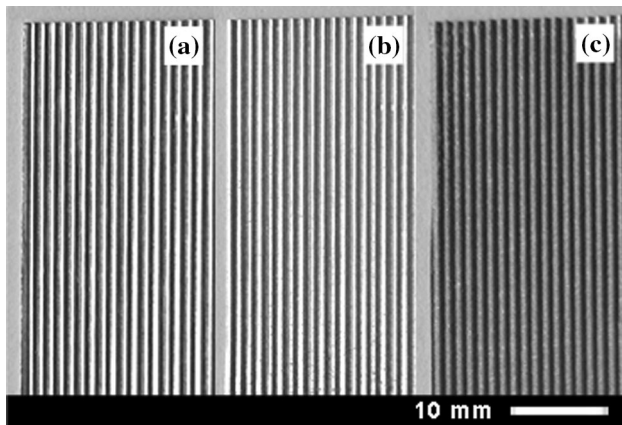
Figure 3 Photographs of the aluminum substrate: (**a**) without treatment (**b**), pretreated with acid for 15 min; (**c**) pretreated with acid for 30 min.

result points a difficulty in the ZIF-8 nucleation onto aluminum and highlights the fact that, in addition to the synthesis parameters, the chemistry of a substrate surface determines the nucleation on it after which the growth could proceed as a continuous film [24]. In order to modify the surface, pretreatments with dilute aqueous solutions of HCl or NaOH were carried out. When aluminum was pretreated with the basic solution up to 30 min or with the acid solution up to 15 min, and then subjected to the solvothermal step, the results were the same and no growth of ZIF-8 developed (Fig. 1c,d). By contrast, and notably, when the acid pretreatment of the substrate extended up to 30 min, a highly crystalline ZIF-8 growth was reproducibly obtained onto the aluminum foil (Fig. 1f), which underlined the determining effect of the substrate surface characteristics in the nucleation and growth of ZIF-8 films. The characteristic ZIF-8 phase confirmed by XRD (Fig. 1e) correlated with the infrared spectrum of this sample (Fig. S1), which showed all the vibration modes of the ZIF-8 structure [2].
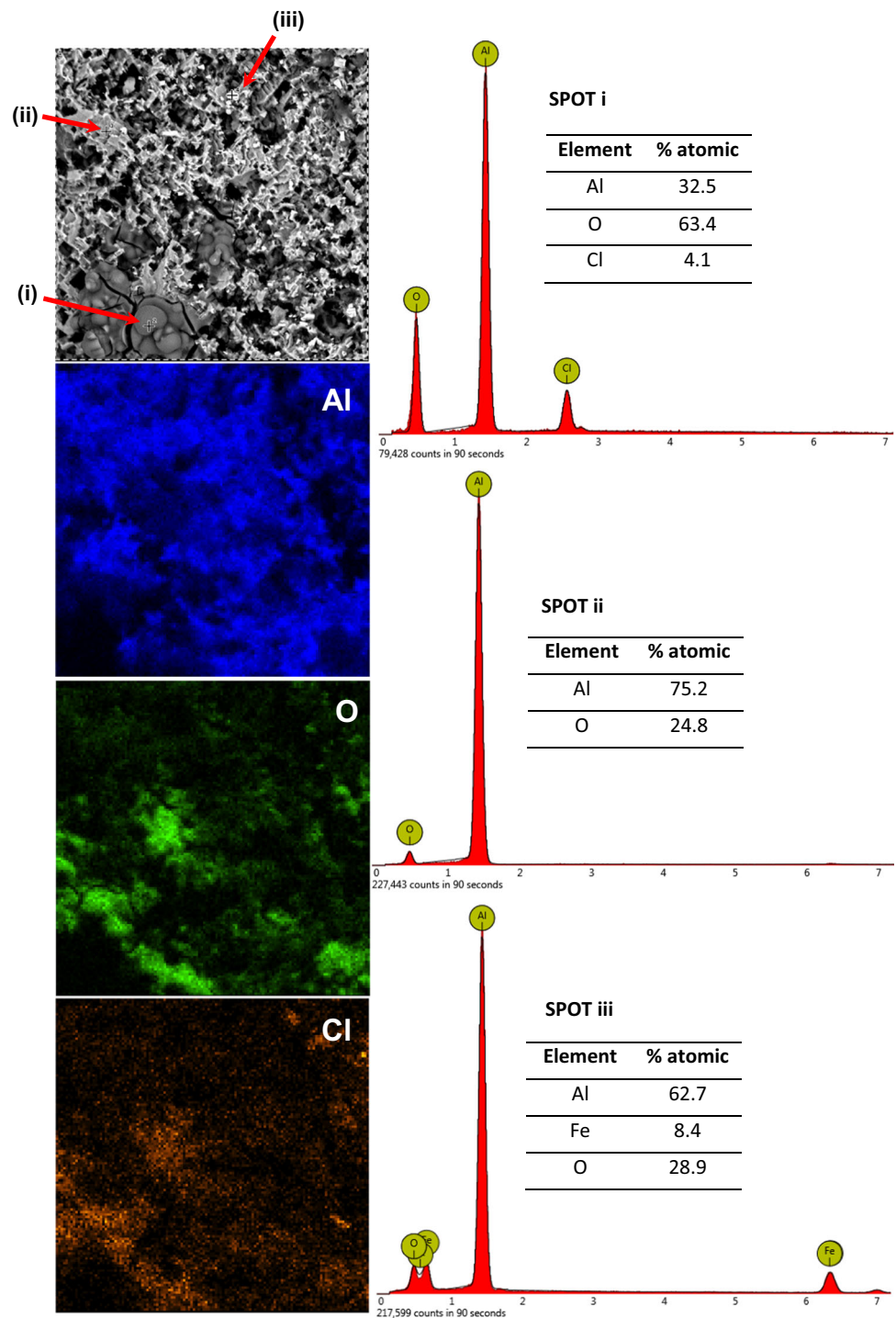
The substrate exhibited a smooth surface (Fig. 2a) with some nanometric indentations most probably due to the micro-folding process. The close-up image in backscattering mode showed particles about 1 μm in size of an element of higher atomic weight embedded at the surface (Fig. 2b). The global EDS analyses indicated a main atomic composition of aluminum and oxygen in line with a surface layer of alumina, added to small amounts of iron which is the main impurity present in this 1050-type aluminum (Fig. S2). When the aluminum was pretreated with

the basic solution, circular craters about 2 microns in size developed with an enrichment in iron and depletion in oxygen, compatible with a leaching of the alumina layer (Fig. S3). Anyway, as shown above, on the substrate thus treated, after the solvothermal step the nucleation of ZIF-8 did not proceed. When the acid pretreatment was applied for 15 min, scattered craters about 5 micron-size, typical of a corrosion process, appeared at the surface (Fig. 2c, d) remaining small amounts of oxygen and iron (Fig. S4), but, as above shown, in this case there was no growth of the MOF either after the solvothermal treatment. On the other hand, when the acid pretreatment extended up to 30 min the substrate turned darker (Fig. 3c), while the corrosion progressed being the surface drastically modified with a gnawed tortuous structure with craters 20–40 μm in size (Fig. 2e). Moreover, formations of a lighter elemental composition with smooth surfaces developed (Fig. 2f) which exhibited an amorphous aspect in agreement with the absence of extra XRD signals in this sample. The global composition indicated a chlorine- and oxygen-rich surface, while punctual analyses clearly showed the elemental distribution (Fig. 4 right); (i) the amorphous structures had a higher content of oxygen and chlorine compatible with an aluminum hydroxychloride phase; (ii) in the sectors of the bulk substrate only aluminum and oxygen were present; (iii) in the regions of bright particles, iron was concentrated. The elemental mapping confirmed the compositional distribution (Fig. 4 left).

Surface characteristics of the substrate

The surface of aluminum showed an Al 2p XPS spectral region with signals at a binding energy (BE) of 74.9 eV that corresponds to aluminum of Al_2O_3 [33] and another at 72.6 eV, compatible with Al^0 (Fig. 5a). Given the superficial nature of this analysis, the presence of metallic aluminum suggests a partial breakdown of the native surface alumina layer, probably during the folding process, exposing some underlying regions of the bulk substrate. This implies that in the pretreatment, the acid must react with both phases. Furthermore, a strong signal in the O 1 s region was observed at 531.6 eV (Fig. 5b), compatible with oxygen of Al_2O_3 [33]. By integrating the signals and considering the response factors of each element, the Al(74.9)/O atomic surface ratio was 0.60 agreeing

Figure 4 EDS analysis of aluminum pretreated with acid for 30 min: on the left, elemental mappings; on the right, punctual elemental analyses in different sectors (spots).

SPOT i

Element	% atomic
Al	32.5
O	63.4
Cl	4.1

SPOT ii

Element	% atomic
Al	75.2
O	24.8

SPOT iii

Element	% atomic
Al	62.7
Fe	8.4
O	28.9

quite well with a superficial layer of alumina (Al/ O = 0.66). In line with the SEM observations, the AFM image of the aluminum showed a smooth surface with maximum height variations of about 12 nm (Fig. 6a), while the analysis in amplitude mode clearly showed the contours of surface g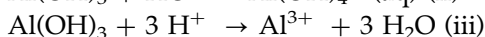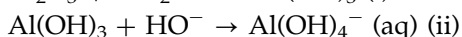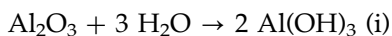rains (Fig. 6b). By contrast, the topographic AFM image of the substrate pretreated with the acid solution for 30 min showed a rougher surface (Fig. 6c), with depressions and ridges up to around 220 nm in height. Furthermore, a nanometric grain structure ($\sim$ 50 nm) was observed which was confirmed in the corresponding amplitude image (Fig. 6d). In addition, in some sectors of this substrate, smoother

Figure 5 XPS of the substrate: (**a**) Al 2p region; (**b**) O 1 s region.
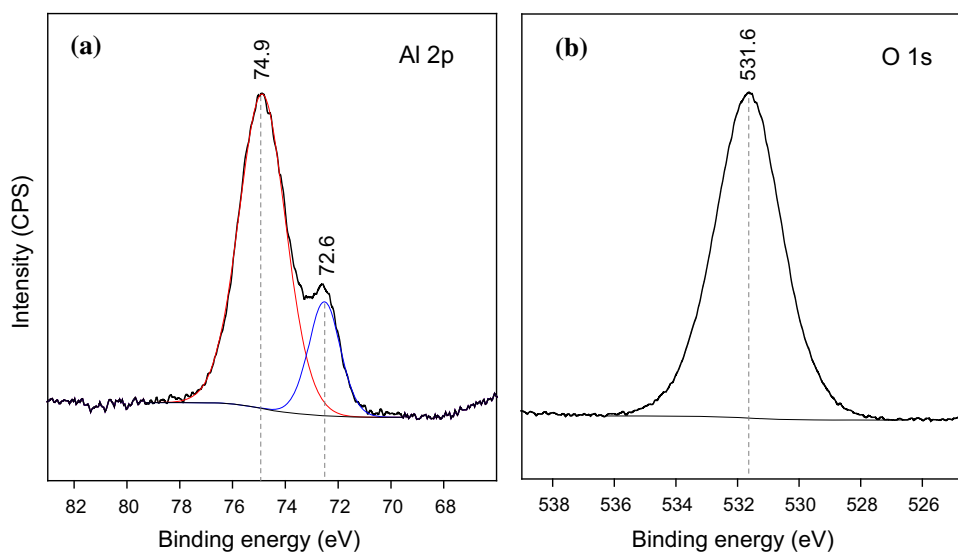

surfaces were detected which contrasted sharply with the grain structure of the aluminum, as can be observed in the amplitude image of Fig. 6e. Likewise, the corresponding phase image (Fig. 6f) confirmed that such regions were of a different chemical nature from that of the substrate (as marked in Fig. 6e,f), proving that they corresponded to the chlorinated phase formed by the acid pretreatment. In this mode, the interaction of the tip of the instrument with the sample produced a change in the phase of the applied sine wave. The registration of the said phase difference is linked to the mechanical and viscoelastic properties of the surface constituents of the material.

The aluminum chemistry indicates that it is spontaneously passivated in air forming a nanometric layer of alumina, boehmite and other partially amorphous phases. Under normal conditions, aluminum reacts slowly with water generating a layer of $Al(OH)_3$ (i), but in a basic (ii) or acidic medium (iii) the said amphoteric layer dissolves [34]:

$$Al_2O_3 + 3\ H_2O \rightarrow 2\ Al(OH)_3\ (i)$$
$$Al(OH)_3 + HO^- \rightarrow Al(OH)_4^-\ (aq)\ (ii)$$
$$Al(OH)_3 + 3\ H^+ \rightarrow Al^{3+} + 3\ H_2O\ (iii)$$

Moreover, in the particular case of contact with an aqueous hydrochloric acid solution, a redox reaction takes place with the aluminum hydroxide, forming aluminum trichloride (iv):

$$3\ HCl(aq) + Al(OH)_3 \rightarrow AlCl_3 + 3\ H_2O\ (iv)$$
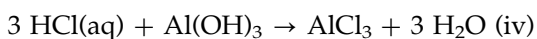
Furthermore, hydrochloric acid has a redox reaction with metallic aluminum, forming aluminum trichloride with evolution of hydrogen (v). During the acid pretreatments, after a certain contact time, a gas evolution was observed:

$$6\ HCl + Al \rightarrow 3\ H_2(g) + 2\ AlCl_3\ (v)$$
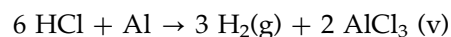
But in reaction (iv), $AlCl_3$ is formed by a stepwise chlorination mechanism where species of aluminum hydroxychlorides $(Al(OH)_nCl_{3-n})$ are produced [35]. Taking into account the evidence of the chlorine- and oxygen-rich phase on the substrate exposed for 30 min to the hydrochloric acid solution, it follows that an aluminum hydroxychloride phase was formed onto this substrate.

Characteristics of the ZIF-8 films

On the acid-pretreated aluminum, a ZIF-8 growth developed as a continuous film that covered all the substrate surface (Fig. 7a). The film exhibited a dense packaging of intergrown crystals that emerged up to the surface with the typical ZIF-8 polyhedral shape, ranging in size from 5 to 8 μm (Fig. 7b). The average total layer thickness was about 10–12 μm (Fig. 7c), with a compact and well-anchored bottom layer at the interface with the substrate (Fig. 7d). The latter allowed a strong anchoring of the ZIF-8 film which was verified because neither detachment nor peeling was observed when subjecting the sample to the ultrasonic bath after the synthesis as well as after the cuttings performed for the SEM studies. The weight gain due to the ZIF-8 growth showed a good reproducibility of the obtained films in several syntheses, being 8.1 ± 0.7 mg per foil. It should also be noted that compact ZIF-8 films of similar characteristics
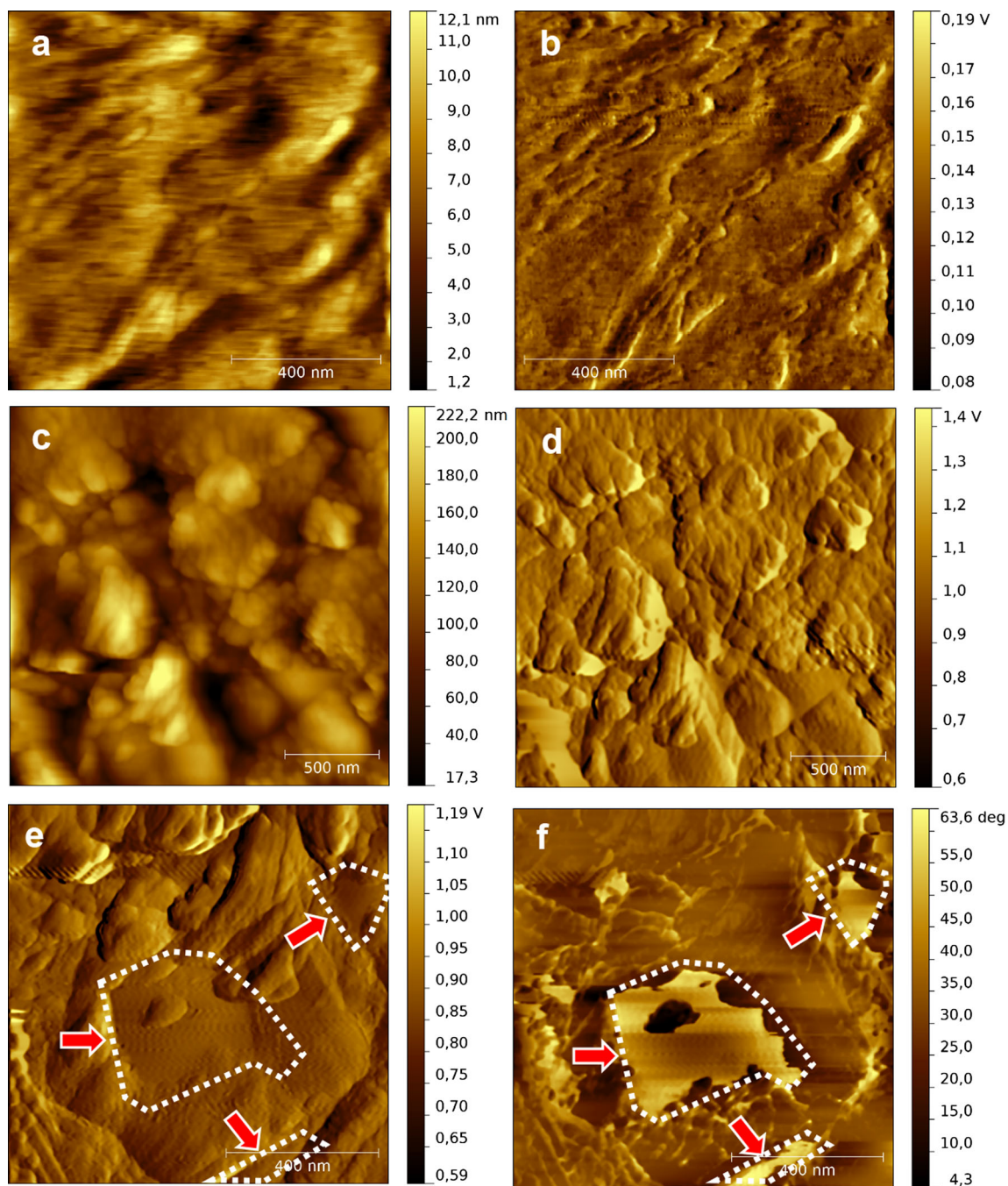
Figure 6 AFM analysis: (**a**) topographic image of the bare substrate; (**b**) amplitude mode image of the bare substrate; (**c**) topographic image of the substrate pretreated with acid for 30 min; (**d**) amplitude mode image of the substrate pretreated with acid for 30 min; (**e**) topographic image of another sector of the substrate pretreated with acid for 30 min; (**f**) amplitude mode image of another sector of the substrate pretreated with acid for 30 min.

were obtained on flat aluminum foils subjected to the same acid pre-treatment (Fig. 7e,f), indicating that with this procedure homogeneous growths can be obtained on substrates of different geometries. ZIF-8/Al films showed high thermal stability, ensuring that

they can be used in applications up to about 400 °C, as shown by the TGA profile obtained from small strips cut from the material (Fig. 8a). Beyond this temperature, the structural collapse of ZIF-8 began due to the linker combustion, similar to that observed

Figure 7 SEM images of ZIF-8 films on aluminum: (**a**) growth in micro-channeled foil; (**b**) close view in hill side area; (**c**) transversal cut; (**d**) close view in transversal cut; (**e**) growth in plain foil; (**f**) close view.
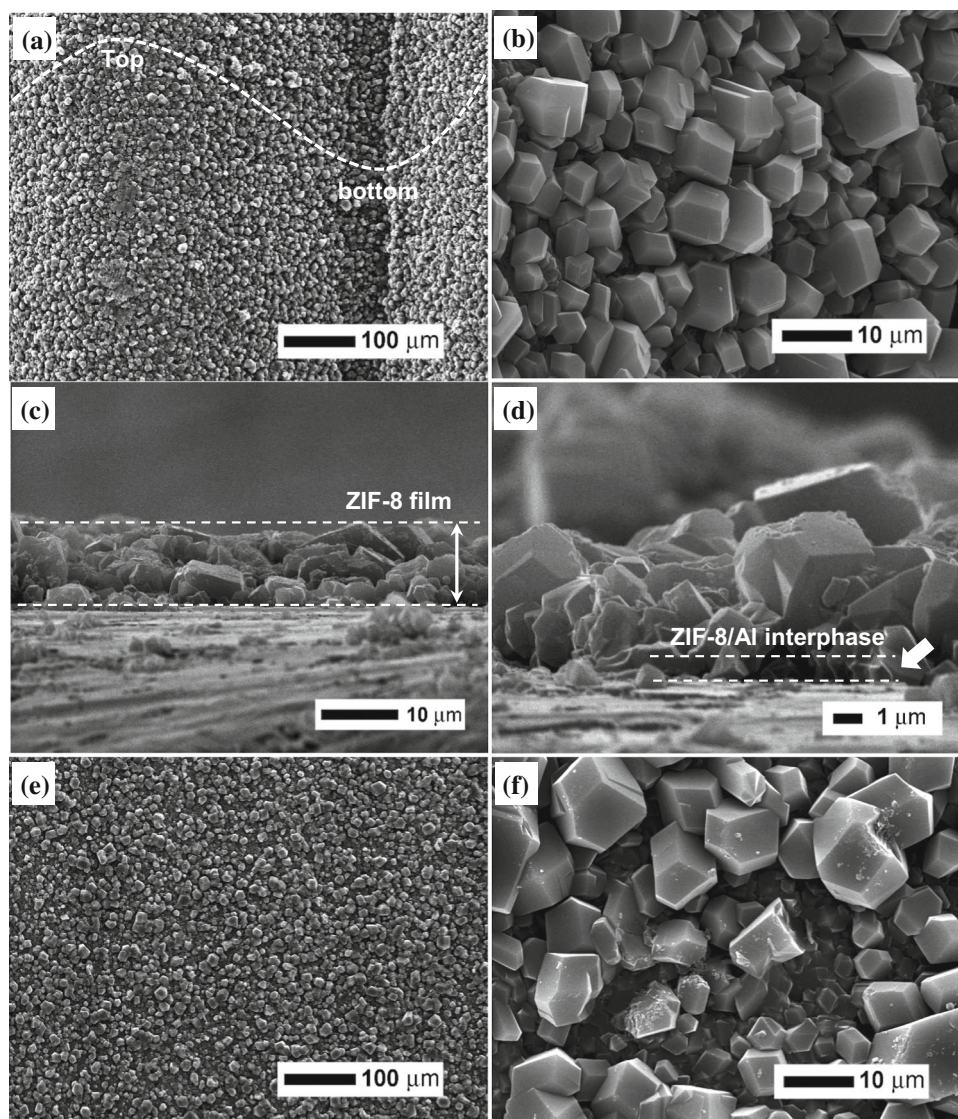
for the recovered powder crystals (Fig. S5). The total mass loss was about 1 wt.%, matching very well with the mass of MOF grown on the substrate, while the structural collapse occurred in two steps at 467 °C and 482 °C (Fig. 8b) as also shown by the exothermic evolutions in the SDTA profiles at the same temperatures (Fig. 8c).

In situ growth mechanism of ZIF-8 onto aluminum

Since both the micro- and nano-topography of the substrate surface was modified with both basic and acid pretreatments as demonstrated by the SEM characterizations, no direct relationship can be established between these properties and the evolution of the ZIF-8 phase, which proceeded in only one case. The most significant difference between all the samples subjected to solvothermal treatments was observed in the substrate pretreated with hydrochloric acid for 30 min. Only in this case, the solvothermal nucleation and growth of a continuous ZIF-8 film proceeded as shown by the SEM, FTIR and XRD studies, while the characterization of the said substrate by SEM–EDS and AFM showed a hydroxychlorinated phase onto its surface. Based on this evidence, it is reasonable to infer that the presence of the said chlorinated phase intervenes in the growth mechanism of the ZIF-8 film, as proposed below. The formation process of ZIF-8 requires the deprotonation of N_1 to form the imidazolate anion, and this step is preceded by the complexation of a
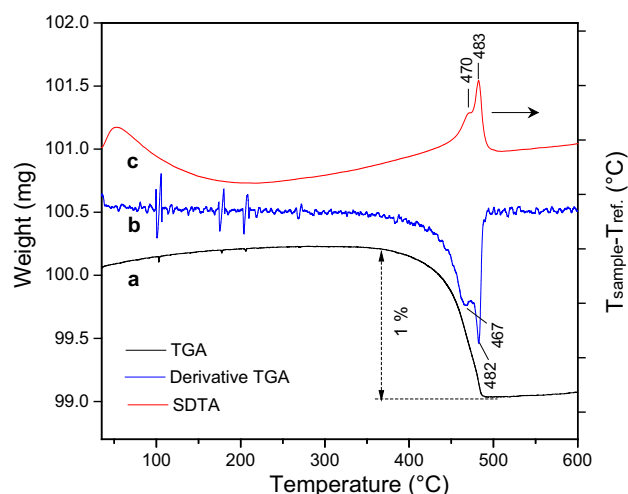
Figure 8 Thermal stability of ZIF-8/Al films: (**a**) TGA profile; (**b**) derivative of TGA; (**c**) SDTA profile.

cation with N_3 which increases the acidity of imidazole [36]. It is evident that the said reactivity onto the surface of the substrate was promoted by the presence of aluminum hydroxychloride sites which are of cationic nature [37]. Then, this favored the binding of 2-methylimidazole to the support surface, polarizing the proton of the pyrimidine group and facilitating the reaction of this group with the Zn^{2+} species present in the reaction medium, which propagates the formation of ZIF-8 nuclei over the aluminum surface. Once the nucleation proceeded, the subsequent anchoring of the growing crystals was promoted by the highly tortuous nature of this substrate surface, which generates a continuous, dense growth of firmly anchored ZIF-8 crystals at the interface with the substrate. The growth mechanism of the ZIF-8 film onto the aluminum foil can be outlined as shown in Fig. 9).

Applied behavior of ZIF-8/Al films

The firmly anchored ZIF-8 films onto the aluminum substrate provide an attractive alternative for those applications that require a fast heat exchange. To evaluate their usefulness, they were doped with platinum and tested in the highly exothermic and model CO oxidation reaction. The objective was not to improve a catalyst formulation for this reaction, but to analyze whether the ZIF-8/Al films could be used in an application with a high thermal demand. It can be observed that Pt(3)/ZIF-8/Al exhibited high activity with a total CO conversion (T^{100}) at 275 °C
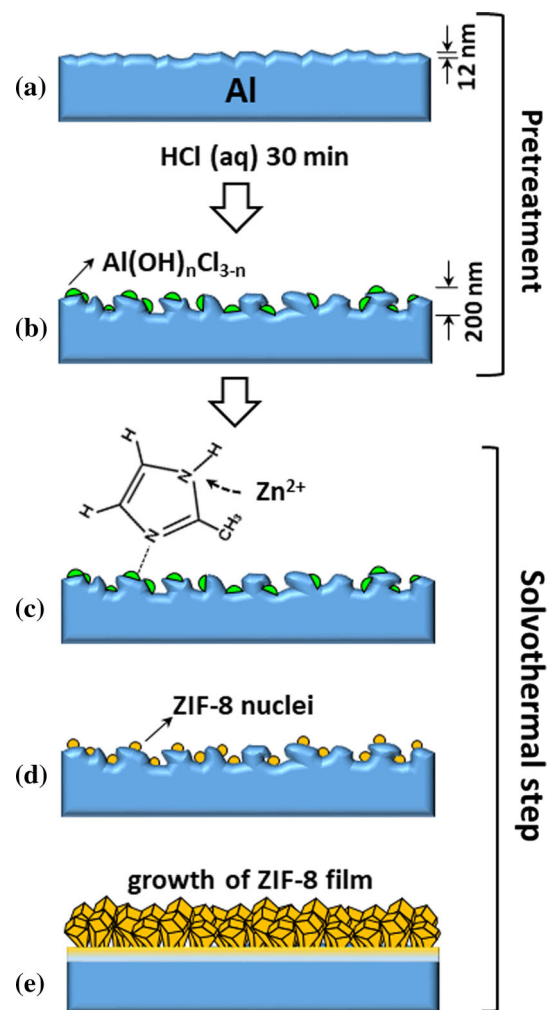

Figure 9 Outline of the ZIF-8 growth on aluminum substrate: (**a**) cleaned substrate; (**b**) pretreatment with HCl solution for 30 min and formation of a surface aluminum oxychloride phase; (**c**) anchoring of 2-methylimidazole to the chlorinated sites; (**d**) nucleation of ZIF-8 at the surface; (**e**) growth of a continuous ZIF-8 film.

and 50% conversion (T^{50}) at 248 °C (Fig. 10), whereas when activation was conducted in H_2, no significant differences were observed (Fig. S6). Considering the Pt-MOF film as the catalytic phase, the said conversions were obtained at a GHSV of 25,000 h^{-1} similar to those reported by Liu et al. for encapsulated Pt clusters within ZIF-8 powder crystals [38]. The activity shown by the films was due to the dispersed platinum species in the ZIF-8 structure, because the MOF by itself is inactive in this reaction [39] and the efficient performance achieved implied a high accessibility of the active species dispersed in the thin film of the MOF.
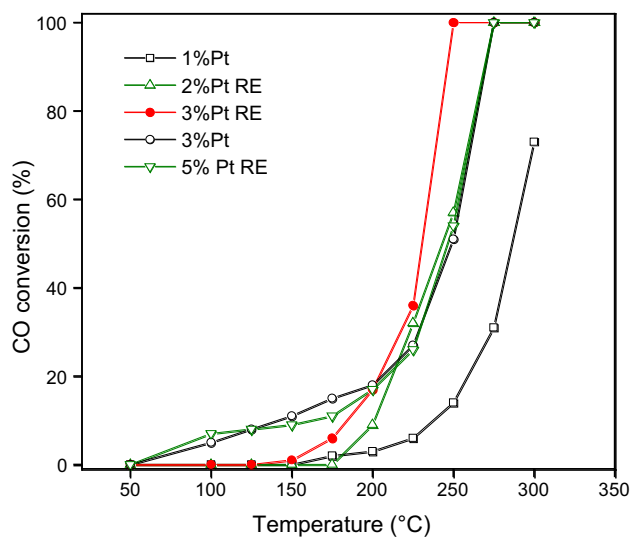
Figure 10 Catalytic behavior of Pt-ZIF-8/Al films in the CO oxidation reaction.
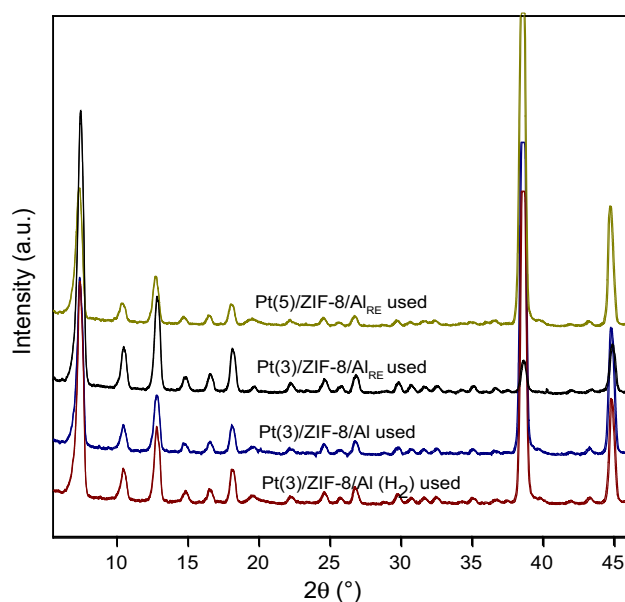

Figure 11 XRD patterns of Pt-ZIF-8/Al films after the catalytic tests.

When the metal loading was lower as in the Pt(1)/ZIF-8/Al sample, the activity decreased (T^{50} 286 °C) highlighting the accessibility and efficient utilization of the dispersed species in the film with the higher metal load (Fig. 10). Then, this sample was disassembled from the microreactor and re-impregnated to obtain the Pt(2)/ZIF-8/Al$_{RE}$ sample which was activated, its activity (T^{50} = 242 °C) being similar to that with 3 wt.% of Pt obtained in a single impregnation step. Then, the same sample was re-

impregnated to obtain a 3 wt.% Pt, activated, and as shown in Fig. 10, this Pt(3)/ZIF-8/Al$_{RE}$ sample exhibited a higher performance than that obtained in a single impregnation step (T^{100} = 250 °C; T^{50} = 230 °C). With consecutive impregnations, more dilute precursor solutions were used allowing a gradual incorporation of small amounts of metal which provided their higher dispersion. However, when the film was re-impregnated up to a 5% wt. loading, the activity decreased a bit because it saturated the dispersion capacity of the MOF. A key feature to be remarked about ZIF-8/Al films is that after the catalytic tests all fully maintained their structural integrity as well as a high Pt dispersion given the absence of its main signal which should be at 2θ 39.8° (JCPDS 4–802) (Fig. 11). It is noteworthy that even in the Pt(3)/ZIF-8/Al$_{RE}$ sample that was subjected to three consecutive catalytic runs, reaching temperatures up to 300 °C, both the ZIF-8 structure and the metallic dispersion were preserved (Fig. 11). The CO oxidation is a highly exothermic reaction (-283 kJ mol^{-1}) in which considerable temperature rises occur within the catalytic phase. Pt-ZIF-8/Al films were stable and maintained their activity over time due to the fast removal of the reaction heat through the highly thermal conductivity substrate, which suppressed the hot spot formation and prevented both the sintering of the active species and the structure of the MOF.

Conclusions

The growth of ZIF-8 films on industrial-type aluminum foils through a low-cost, easy methodology employing a direct solvothermal treatment was obtained. To achieve the film growth, it was only necessary to treat the substrate by a short (30 min) contact with a dilute (5%wt.) hydrochloric acid solution which produced a highly tortuous surface with aluminum hydroxychloride-type sites that induced the solvothermal nucleation and growth of the MOF. The applied methodology is very simple and fast, avoiding long and expensive procedures, and represents a new contribution to the current state of knowledge in the field of ZIF-8 coatings. The obtained ZIF-8 films were homogeneous, continuous, about 10 μm in thickness and exhibited a compact inter-grown and highly adherent layer in tight contact at the film/substrate interface. Moreover, it was

shown that such ZIF-8/Al films are effective for use in a highly exothermic process such as the CO oxidation reaction, avoiding the sintering of dispersed active phases and preserving the structural integrity of the MOF after repeated reaction cycles. The results achieved are encouraging to move forward in the use of ZIF-8/Al films for applications at moderate temperatures in which a fast thermal response can be a critical factor.

Acknowledgments

Compliance with ethical standards

Conflict of interest The authors declare that they have no conflict of interest.

Supplementary material Complementary results of characterization related to this article by FTIR, SEM, EDS, TGA and catalytic assay are provided.Supplementary file1 (PDF 2.21 mb)

Supplementary information: The online version contains supplementary material available at (http s://doi.org/10.1007/s10853-021-05850-0)

References

[1] Phan A, Doonan C, Uribe-Romo F, Knobler C, O'Keeffe M, Yaghi O (2010) Synthesis, structure, and carbon dioxide capture properties of zeolitic imidazolate frameworks. Acc Chem Res 43:58–67

[2] Park K, Ni Z, Coté A, Choi J, Huang R, Uribe-Romo F, Chae H, O´Keeffe M, Yagui O, (2006) Exceptional chemical and thermal stability of zeolitic imidazolate frameworks. PNAS 103:10186

[3] Yao J, Wang H (2014) Zeolitic imidazolate framework composite membranes and thin films: synthesis and applications. Chem Soc Rev 43(13):4470–4493

[4] Bux H, Feldhoff A, Cravillon J, Wiebcke M, Li Y-S, Caro J (2011) Oriented zeolitic imidazolate framework-8 membrane with sharp H_2/C_3H_8 molecular sieve separation. Chem Mater 23:2262–2269

[5] Kwon H, Jeong H-K (2013) In Situ Synthesis of thin zeolitic-imidazolate framework ZIF-8 membranes exhibiting exceptionally high propylene/propane separation. J Am Chem Soc 135(29):10763–10768

[6] Venna S, Carreon M (2009) Highly Permeable zeolite imidazolate Framework-8 MEMBRANES for CO_2/CH_4 separation. J Am Chem Soc 132:76–78

[7] Betard A, Fischer R (2012) Metal-organic framework thin films: from fundamentals to applications. Chem Rev 112:1055–1083

[8] Kida K, Fujita K, Shimada T, Tanaka S, Miyake Y (2013) Layer-by-layer aqueous rapid synthesis of ZIF-8 films on a reactive surface. Dalt Trans 42(31):11128–11136

[9] Chen L-J, Luo B, Li W-S, Yang YT, Li S-S, Wang X-Z, Cui Y-J, Li H-Y, Qian G-D (2016) Growth and characterization of zeolitic imidazolate framework-8 nanocrystalline layers on microstructured surfaces for liquid crystal alignment. RSC Adv 6:7488

[10] He M, Yao J, Li L, Zhong Z, Chen F, Wang H (2013) Aqueous solution synthesis of ZIF-8 films on a porous nylon substrate by contra-diffusion method. Micropor Mesopor Mater 179:10–16

[11] Hamid M, Park S, Kim J, Lee Y, Jeong H-K (2019) In-Situ formation of Zeolitic-Imidazolate framework thin films and composites using modified polymer substrates. J Mater Chem A 7:9680–9689

[12] Dumée L, He L, Hill M, Zhu B, Duke M, Schütz J, She F, Wang H, Gray S, Hodgsona P, Kong L (2013) Seeded growth of ZIF-8 on the surface of carbon nanotubes towards self-supporting gas separation membranes. J Mater Chem A 1(32):9208–9214

[13] Bux H, Chmelik C, Krishna R, Caro J (2011) Ethene/ethane separation by the MOF membrane ZIF-8: Molecular correlation of permeation, adsorption, diffusion. J Memb Sci 369(1–2):284–289

[14] Tian F, Cerro AM, Mosier AM, Wayment-Steele HK, Shine RS, Park A, Webster ER, Johnson LE, Johal MS, Benz L (2014) Surface and stability characterization of a nanoporous ZIF-8 thin film. J Phys Chem C 118(26):14449–14456

[15] Chocarro-Ruiz B, Pérez-Carvajal P, Avci C, Calvo-Lozano O, Alonso M, Maspoch D, Lechuga L (2018) A CO2 optical sensor based on self-assembled metal–organic framework nanoparticles. J Mater Chem A 6:13171

[16] Segovia G, Tuninetti J, Moya S, Picco A, Ceolín M, Azzaroni O, Rafti M (2018) Cysteamine-modified ZIF-8 colloidal building blocks: direct assembly of nanoparticulate MOF

films on gold surfaces via thiol chemistry. Mat Today Chem 8:29–35

[17] Makiura R, Motoyama S, Umemura Y, Yamanaka H, Sakata O, Kitagawa H (2010) Surface nano-architecture of a metal-organic framework. Nat Mater 9:565

[18] Stassen I, Styles M, Grenci G, Van Gorp H, Vanderlinden W, De Feyter S, Falcaro P, De Vos D, Vereecken P, Ameloot R (2016) Chemical vapour deposition of zeolitic imidazolate framework thin films. Nature Mater 15:304–310

[19] Kim D-Y, Joshi B, Lee J-G, Lee J-H, Lee J-S, Hwang Y, Chang J-S, Al-Deyab S, Tan J-C, Yoon S (2016) Supersonic cold spraying for zeolitic metal–organic framework films. Chem Eng J 295:49–56

[20] Fischer D, von Mankowski A, Ranft A, Vasa S, Linser R, Mannhart J, Lotsch B (2017) ZIF-8 films prepared by femtosecond pulsed-laser deposition. Chem Mater 29:5148–5155

[21] Huang A, Liu Q, Wang N, Caro J (2014) Highly hydrogen permselective ZIF-8 membranes supported on polydopamine functionalized macroporous stainless-steel nets. J Mater Chem A 2(22):8246–8251

[22] Ma Q, Li G, Liu X, Wang Z, Song Z, Wang H (2018) Zeolitic imidazolate framework-8 film coated stainless steel meshes for highly efficient oil/water separation. Chem Commun 54:5530–5533

[23] Ji H, Hwang S, Kim K, Kim C, Jeong N (2016) Direct in Situ conversion of metals into metal−organic frameworks: a strategy for the rapid growth of mof films on metal substrates. ACS Appl Mater Interfaces 8:32414–32420

[24] Papporello R, Miró E, Zamaro J (2015) Secondary growth of ZIF-8 films onto copper-based foils. Insight into surface interactions. Micropor Mesopor Mater 211:64–72

[25] Touloukian, Y.S., Powell, R.W., Ho, C.Y., Klemens, P.G.: Thermophysical properties of matter-the TPRC Data. In: Thermal Conductivity-Metallic Elements and Alloys, vol. 1, SBN 306–67021–6. IFI/Plenum, New York, Washington (1970)

[26] Boger T, Heibel AK (2005) Heat transfer in conductive monolith structures. Chem Eng Sci 60(7):1823–1835

[27] Papurello R, Fernández J, Miró E, Zamaro J (2017) Microreactor with silver-loaded metal-organic framework films for gas-phase reactions. Chem Eng J 313:1468–1476

[28] Cui B, Audu CO, Liao Y, Nguyen ST, Farha OK, Hupp JT, Grayson M (2017) Thermal conductivity of ZIF-8 thin-film under ambient gas pressure. ACS Appl Mater Interfaces 9:28139–28143

[29] Zhang J, Ramachandran PV, Gore JP, Mudawar I, Fisher TS (2005) A review of heat transfer issues in hydrogen storage technologies. J Heat Transfer 127(12):1391–1399

[30] Zhang M, Ma L, Wang L, Sun Y, Liu Y (2018) Insights into the use of metal−organic framework as high-performance anticorrosion coatings. ACS Appl Mater Interfaces 10:2259–2263

[31] Zhang M, Liu Y (2020) Enhancing the anti-corrosion performance of ZIF-8-based coatings via microstructural optimization. New J Chem 44:2941–2946

[32] Hernandez J, Choren E (1983) Thermal stability of some platinum complexes. Thermochim Acta 71(3):265–272

[33] Reddy N, Bera P, Reddy V, Sridhara N, Dey A, Anandan C, Sharma A (2015) XPS study of sputtered alumina thin films. Ceram Int 40(7):11099–11107

[34] Kaesche H (2003) Corrosion of metal. Springer-Verlag, Berlin Heidelberg, Physicochemical Principles and Current Problems

[35] Leygraf C, Graede T (2000) Atmospheric corrosion. Inc, New York

[36] Fernández-Bertrán J, Castellanos-Serra L, Madeira H, Reguera E (1999) Proton transfer in solid state: mechanochemical reactions of imidazole with metallic oxides. J Solid State Chem 147:561–564

[37] Teagarden DL, Radavich JF, White J, Hem SL (1981) Aluminum chlorohydrate 11: physicochemical properties. J Pharm Sci 70(7):762–764

[38] Wang P, Liu J, Liu C, Zheng B, Zou X, Jia M, Zhu G (2016) Electrochemical synthesis and catalytic properties of encapsulated metal clusters within zeolitic imidazolate frameworks. Chem Eur J 122:16613–16620

[39] Jiang H, Liu B, Akita T, Haruta M, Sakurai H, Xu Q (2009) Au@ZIF-8: CO Oxidation over gold nanoparticles deposited to metal−organic framework. J Am Chem Soc 131:11302–11303